Int. J. Electrochem. Sci., 7 **(2012)** 12181 - 12192

International Journal of
ELECTROCHEMICAL
SCIENCE
www.electrochemsci.org

Computational Fluid Dynamics Characterization of a Rotating Cylinder Electrochemical Reactor using an RANS-RNG Turbulence Model

R. Enciso, L. A. Padilla, C. Ojeda, J. A. Delgadillo, I. Rodríguez[*]

Facultad de Ingeniería-Instituto de Metalurgia, Universidad Autónoma de San Luis Potosí. Av. Sierra Leona 550 Lomas 2ª sección, 78210 San Luis Potosí, México.
*E-mail: learsi@uaslp.mx

Received: 5 October 2012 / *Accepted:* 22 October 2012 / *Published:* 1 December 2012

The electrochemical reactor with a rotating cylinder electrode is typically used in processes under mass transfer control. Characterization of the flow is needed to optimize the efficiency of the reactor. Because the complexity of the geometry in 3 dimensions requires a more sophisticated approach, computational fluid dynamics (CFD) has been used to describe the fluid flow in a 3-dimensional electrochemical rotating cylinder reactor. CFD has been applied in some studies, but these studies have not addressed the effect of the counter electrode geometry. In this paper, a CFD description of an electrochemical rotating cylinder reactor with four plates as counter electrodes is presented. Four design configurations were explored, in which both the size and number of counter electrodes were varied. The rotation velocity of the cylinder electrode was held constant at 400 rpm. The software Fluent™ was used to solve the governing equations, and the RNG k-ε model was used to describe the turbulence effect of the flow. The simulated results were validated with experimental data obtained by digital image analysis (DIA) at the surface of the reactor. The results show that the arrangement of the electrode and counter electrodes significantly modifies the stream lines of the flow, generating high-velocity zones within the tank of the reactor, particularly at the surface of the electrode and at the bottom of the reactor. Furthermore, there are some zones at the periphery of the electrodes that exhibit low-velocity stream lines. The experimental profiles are described with CFD modeling and demonstrate the validity of the models used in the simulation. Therefore, full characterization of the fluid flow of an electrochemical reactor is possible through the application of CFD.

Keywords: computational fluid dynamics, rotating cylinder electrode, digital image analysis.

1. INTRODUCTION

Electrochemical rotating cylinder reactors are frequently used to remove heavy metals from dilute industrial effluents and in the treatment of water by electrochemical reduction of metals, such as

cadmium [1], copper [2], zinc [3], and chromium [4]. The complexity of the reactor's geometry makes it difficult to fully describe the internal stream lines, but because the efficiency of the reactor is closely related with the dynamics of the flow, an adequate description of the stream lines is needed. Rivera et al. [5] showed that an important effect exists when the gap of the counter electrode is changed and concluded that the hydrodynamics of the flow modifies the mass transport in the reactor. Therefore, a full characterization of the flow is needed to optimize the reactor design and efficiency of the process.

Computational fluid dynamics (CFD) has been used to describe a wide range of processes and to develop new technology. In particular, the computational tool is often used to describe electrochemical reactors [6 - 9] in which the dynamics of the flow can be described accurately. The description of the turbulence closure model is mandatory for an acceptable characterization of the flow, and the most direct approach is the experimental evaluation of the dynamics of the flow inside the reactor.

Tomasoni et al. [10] characterized the transport phenomena of an electrochemical rotating cylinder reactor using a combination of experimental, numerical and theoretical approaches. The experimental velocity profiles were obtained with particle image velocimetry (PIV), and the results of the simulation were compared using 2 dimensions Reynolds-averaged Navier–Stokes equations (RANS) and Direct Numerical simulation (DNS). While the DNS solution is more expensive, it describes all of the energy scales of the flow, showing good agreement with experimental data. Tomasoni et al. [10] did not present the validation of the RANS approach because they used a 2 dimensions solution with a standard κ-ε model. The standard κ-ε model is appropriate for predicting flows with low curvature, whereas when the curvature increases, the RNG κ-ε model is more accurate for capturing the turbulence fluctuation of swirl flows [11].

Rivero et al. [6] applied the RANS approach in 3 dimensions to model the hydrodynamic behavior of an RCE. The simulated results were validated by modeling the kinetics of copper recovery, showing good agreement with the experimental data.

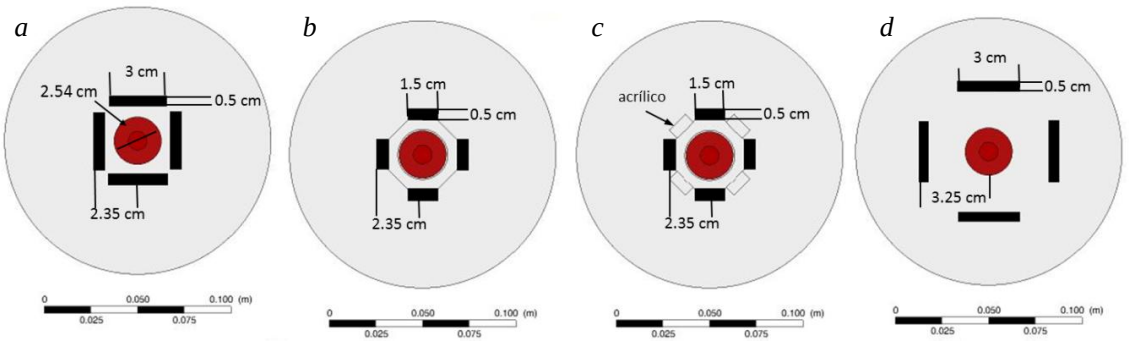

Figure 1. Top view of the RCE reactor, where the black plates are the counter electrodes, the white plates are the acrylic plates, and the orange circle is the copper cylinder.

In the rotating cylinder reactor, the curvature of the stream lines requires a different turbulence model and a 3-dimensional solution. Thus, in the present paper, the flow is characterized using the FLUENT^{TM} software by applying an RNG κ-ε model with a correction for curvature to provide

turbulence closure and accounting for several counter electrode configurations. The simulated results were compared with experimental stream lines obtained with digital image analysis of the actual flow. The size and number of plates used as counter electrodes around a copper cylinder were set up in 4 different geometries, as shown in Figure 1.The system was modeled in 3 dimensions. The dimensions of the reactor are shown in Figure 2. The plates and counter electrodes can be configured in different ways using the same reactor.

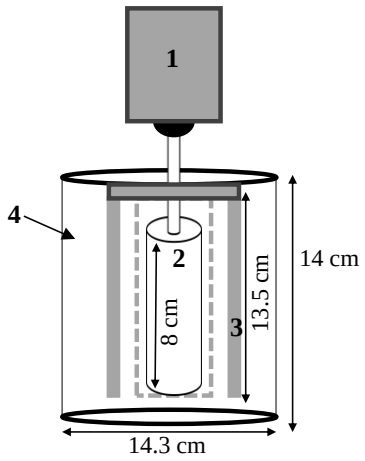

Figure 2. Dimensions of the reactor in mm. 1) Rotor, 2) Copper cylinder, 3) Acrylic plates, 4) Reactor frame.

2. MODELING

The modeling was performed using the code ANSYS 14.0, where Fluent^{TM} is used to compute the governing equations of the fluid as well as the mass balance, momentum balance and turbulence effect. The governing equations are the continuity and Navier-Stokes equations in 3 dimensions and thus require significant computational effort. The solution of these equations and the turbulence effect are performed with computational fluid dynamics (CFD). The mass balance is described by the continuity equation shown in Equation (1).

$$\frac{\partial \rho}{\partial t} + \rho \frac{\partial u_i}{\partial x_i} = 0 \qquad (1)$$

The momentum balance is described by the Navier-Stokes equations, as shown in Equation (2).

$$\frac{\partial (\rho u_i)}{\partial t} + \frac{\partial (\rho u_i u_j)}{\partial x_j} = -\frac{\partial \rho}{\partial x_i} + \frac{\partial}{\partial x_j}\left(\mu \frac{\partial u_i}{\partial x_j} \right) + \rho g_i \qquad (2)$$

Equations (1) and (2) are nonlinear partial differential equations in 3 dimensions and thus require

discretization of the domain with a mesh, which is independent of the solution. To reduce the computational time, the velocity is decomposed into its mean and fluctuating components. The resulting equations for incompressible fluids are shown in Equations (3) and (4). Consequently, these equations describe the mean velocity field that can be resolved with a coarser mesh. The governing equations for the velocity field in an incompressible fluid can be written according to Equations (2) and (3) when the velocity (u_i) is described by its mean $\left(\langle u_i \rangle\right)$, and fluctuation $\left(u_i'\right)$ (Equation (3)).

$$u_i = \langle u_i \rangle + u_i' \tag{3}$$

$$\frac{\partial \rho}{\partial t} + \rho \frac{\partial \langle u_i \rangle}{\partial x_i} = 0 \tag{4}$$

$$\frac{\partial \left(\rho \langle u_i \rangle\right)}{\partial t} + \frac{\partial \left(\rho \langle u_i \rangle \langle u_j \rangle\right)}{\partial x_j} = -\frac{\partial (\rho)}{\partial x_i} + \frac{\partial}{\partial x_j}\left(\mu \frac{\partial \langle u_i \rangle}{\partial x_j}\right) + \frac{\partial}{\partial x_j}\left(-\rho \langle u_i' u_j' \rangle\right) + \rho g_i \tag{5}$$

Here, the term $-\rho \langle u_i' u_j' \rangle$ includes the turbulence effect, which must be modeled to solve Equation (5). Different models have been used to describe this term. In this paper, the RNG κ-ε model is used because it has been shown to be more accurate for capturing the turbulence fluctuation of swirl flows [11], as is present in the rotating cylinder. The standard κ-ε model has been successfully used in different electrochemical reactors [7] in which the flow is not rotating.

The renormalization group (RNG) κ-ε model is similar in form to the standard κ-ε model but includes additional terms for the dissipation rate ε development, which significantly improves the accuracy of the model, particularly for rapidly strained flows. The effect of swirl on turbulence is included in the RNG model, enhancing the accuracy for swirling flows. These advantages make the RNG κ-ε model more accurate and reliable for describing the flow than the standard κ-ε model. The RNG κ-ε model describes the term $-\rho \langle u_i' u_j' \rangle$ as

$$-\rho \langle u_i' u_j' \rangle = \mu_t \left(\frac{\partial u_i}{\partial x_j} + \frac{\partial u_j}{\partial x_i}\right) \tag{6}$$

where μ_t is the turbulent viscosity, which is directly related to the turbulent kinetic energy and viscous dissipation, ε, as follows:

$$\mu_t = \rho C_\mu \frac{k^2}{\varepsilon} \tag{7}$$

The kinetic energy and dissipation rate are obtained from the transport equations given below.

$$\frac{\partial}{\partial t}(\rho k)+\frac{\partial}{\partial x_i}(\rho k u_i)=\frac{\partial}{\partial x_j}\left(\alpha_k \mu_{eff}\frac{\partial k}{\partial x_j}\right)+2\mu_t S_{ij}S_{ij}-\rho\varepsilon \quad (8)$$

$$\frac{\partial}{\partial t}(\rho \varepsilon)+\frac{\partial}{\partial x_i}(\rho \varepsilon u_i)=\frac{\partial}{\partial x_j}\left(\alpha_\varepsilon \mu_{eff}\frac{\partial \varepsilon}{\partial x_j}\right)+C_{1\varepsilon}\frac{\varepsilon}{k}\left(2\mu_t S_{ij}S_{ij}\right)-C_{2\varepsilon}\rho\frac{\varepsilon^2}{k}-\frac{C_\mu \rho \eta^3\left(1-\eta/\eta_0\right)}{1+\beta\eta^3}\frac{\varepsilon^2}{\kappa} \quad (9)$$

where C_μ = 0.0845 is derived from renormalization group methods [12], μ_{eff} is the effective viscosity, which is defined as the summation of μ and μ_2, and α_κ and α_ε are the inverse effective Prandtl number for κ and ε, respectively. The mean strain rate, S_{ij}, is expressed as

$$S_{ij}=\frac{1}{2}\left(\frac{\partial u_i}{\partial x_j}+\frac{\partial u_j}{\partial x_i}\right) \quad (10)$$

The term $C_\mu\rho\eta^3(1-\eta/\eta_0)\varepsilon^2)/(1+\beta\eta^3)$ (ε^2/κ) is the main difference between the standard κ-ε model and RNG κ-ε model. When the rate strain, S_{ij}, is large ($\eta > \eta_0$), this term makes a negative contribution. Compared to the standard κ-ε, there is a smaller destruction of ε, which eventually reduces the effective viscosity. As a result, in rapidly strained flows, the RNG model yields a lower turbulent viscosity than the standard κ-ε model. The RNG model is more responsive to the effects of rapid strain and streamline curvature than the standard κ-ε model, which explains the better performance of the RNG model for rotating reactor flows. The use of μ_{eff} allows the model to better handle low Reynolds numbers and near wall flows.

2.1 Interface modeling

At the top of the reactor, the fluid is in contact with air, forming a free surface interface. The interface modeling is very important because the free movement of the flow is determined by the boundaries of the system. The volume of fluid (VOF) model was used to describe the shape and momentum transfer at the interface. The volume of fluid (VOF) model was used to compute the interaction between the air and water phases. The nature of the interface is unsteady [13], and the tracking is by the solution of the continuity equation shown in Equation 11.

$$\frac{\partial \alpha_\gamma}{\partial t}+u_i\frac{\partial \alpha_\gamma}{\partial x_i}=0 \quad (11)$$

where α_γ is the volume fraction of the phase. The properties in any given cell are representative of the fraction of air α_γ in the air and water mixture for any f property of two phases; the volume fraction of the property is taken from Equation 12.

$$f = \sum_{\gamma=1}^{\gamma=2} \alpha_\gamma f_\gamma \qquad (12)$$

In this manner, density and viscosity can be computed for each cell throughout the domain. The corresponding momentum equation is solved with the average density and viscosity of the interface. The resulting velocity field is shared between the two phases to provide a calculated boundary condition at the interface.

3. REACTOR DOMAIN AND MESHING OF THE SYSTEM

The reactor domain was divided into 2 parts to generate a stable and independent mesh. The first section is the rotating electrode and counter electrodes, and the second section is the tank where the electrolyte is present. The separation of the two sections allowed for the construction of a better mesh. An independent solution of the mesh was obtained, and the size of the mesh was changed until the solution did not vary for each reactor arrangement. Table 1 presents the number elements, nodes and skewness for each reactor. A good-quality mesh should have a skewness factor above 95%. In mesh *c*, the maximum skewness factor achieved was 94.25%. However, the solution was stable, so the mesh was used.

Table 1. Mesh quality of the reactors.

Reactor Type	Elements	Nodes	Skewness factor
a	440,847	81,601	98.92%
b	174,025	35,156	96.02%
c	193,640	39,369	94.25%
d	442,531	81,891	97.85%

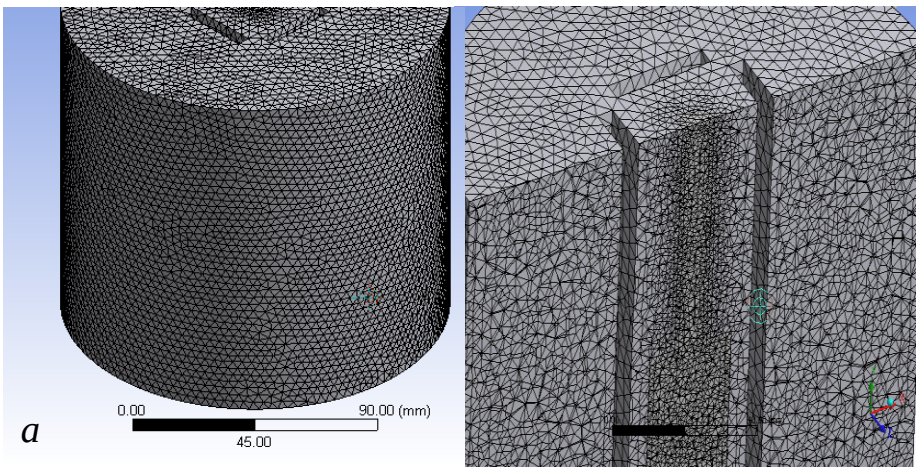

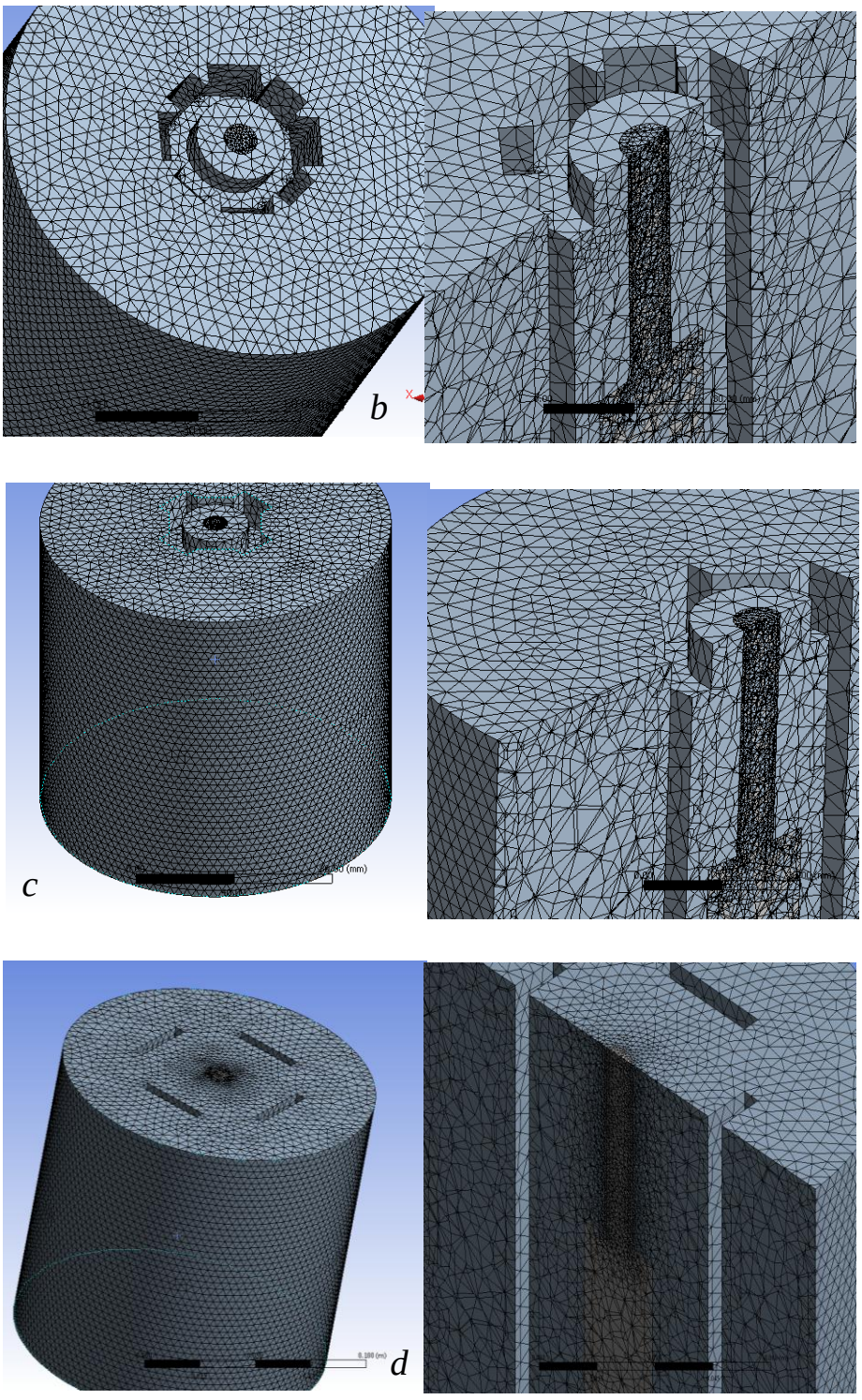

Figure 4. Unstructured mesh characteristics for each reactor configuration.

Figure 3 shows the four unstructured meshes used for each reactor, where the number of elements and nodes are described in Table 1. The main concentration of the element is in the copper electrode. The mesh in each case was tested to be independent of the solution.

4. SIMULATED RESULTS AND VALIDATION

The solution of the Navier-Stokes equations, VOF modeling of the interface and the turbulence closure model RNG κ-ε were performed using the code Fluent™ in a workstation Dell™ Precision T7500 with a processor Intel®Xeon® CPU x5482 3.20 GHz 16 GB RAM. The computing time to simulate the rotation of the fluid was of approximately 8 hours for each reactor.

4.1 Boundary conditions

The system was defined as a static wall in the reactor and counter electrodes, and in the top of the reactor, the system was defined as a pressure outlet of 1 atm. The copper cylinder was defined as a moving reference frame wall spinning at 400 rpm in contact with the electrolyte. An interface was defined at the boundary of the electrolyte and air, as shown in Figure 5.

The definition of this interface is very important because this definition allows for a free flow of the fluid imposed by the rotating cylinder. The momentum is transferred between the interface, and the equations are solved for the air and electrolyte section. The electrolyte was defined as pure water.

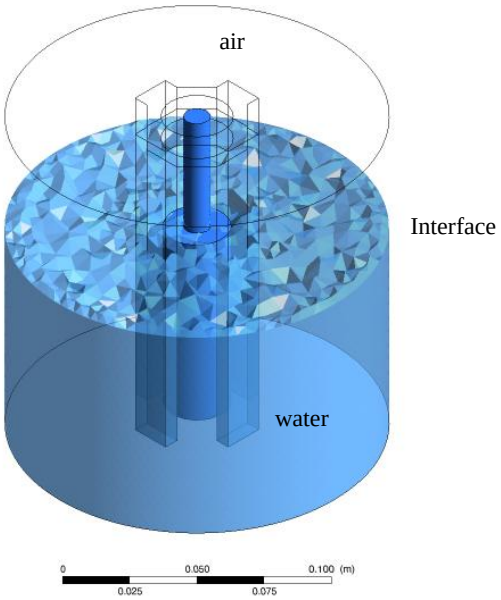

Figure 5. Interface location in the reactor.

4.2 Experimental validation

Experimental results were used to validate the simulated data. The experimental stream lines were calculated using the digital image analysis (DIA) technique. Each configuration was loaded with electrolyte and 50 micrometers polymeric particles as tracers, and the rotating cylinder was set at 400 rpm. For each reactor configuration, a video was taken using a Canon GL 3CCD NTSC video camera to record slow-motion videos with a speed of 1/2,400 s.

The video was sectioned into frames to trace the polymeric particles suspended in the fluid to calculate the trajectory of the stream lines for each reactor configuration. After the 4 videos were generated, the Free Studio Manager 4.3.5.75 software was used to convert the video into timed frames. Then, the timed images generated from the videos were analyzed with the open-source software Image J to calculate the stream lines of the fluid tracking the trajectory of polymeric particles suspended in the electrolyte.

In Figure 6, the reactor with configuration *a* is presented and compared with the simulated and experimental profiles. Figure 6(a) shows the stream lines of the flow along the *y* axis. The electrolyte is driven out to the inter-electrode zone through the gaps. Figure 6 (b) shows the stream lines of the flow using DIA, and the results indicate that the flow field is properly represented.

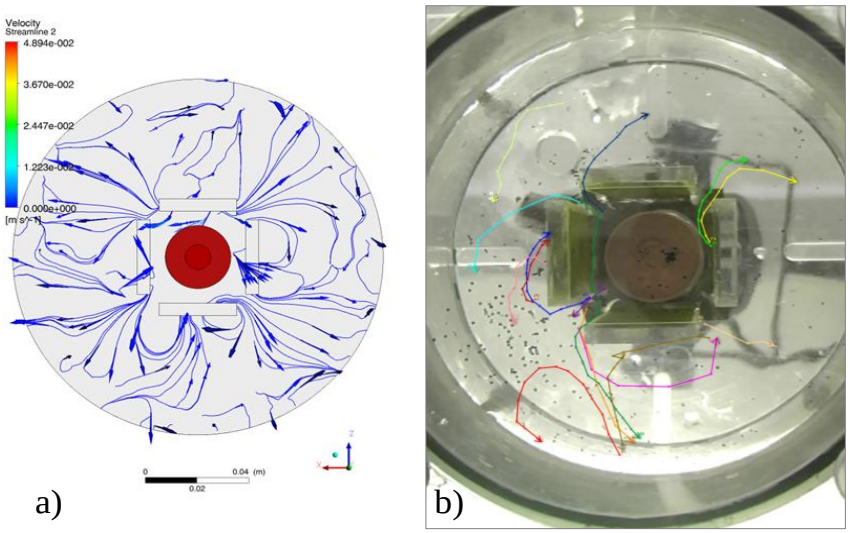

Figure 6. Stream lines for reactor *a*.

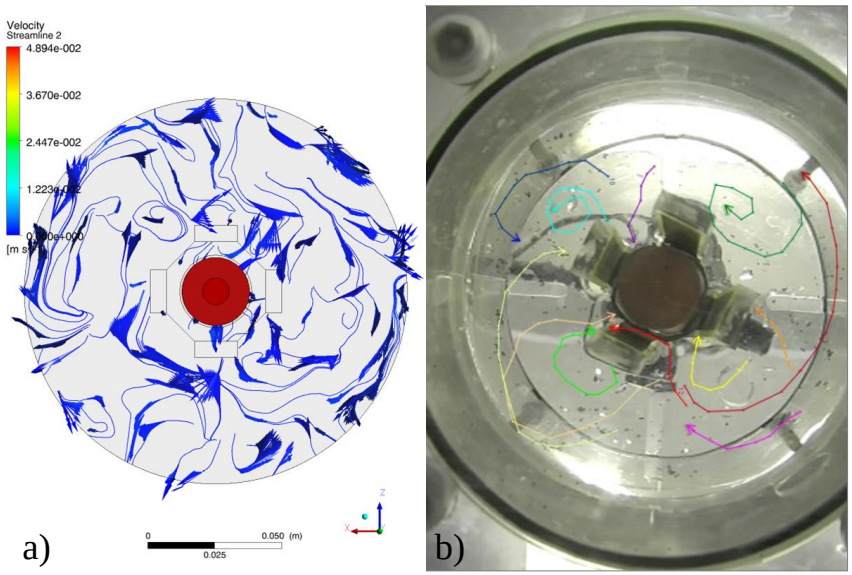

Figure 7. Stream lines for reactor *b*.

The simulated and experimental flow fields of reactor *b* are shown in Figure 7. In this case, the gap between the counter electrodes is increased, and the electrolyte can flow easily. The stream lines show that as the copper electrode spins, the electrolyte is driven towards the electrode zone, modifying the dynamics of the flow and the electrical characteristics of the reactor.

Another important modification is the volume of fluid in the space between the counter electrode and copper electrode. In reactor *c*, inert acrylic plates were placed between the inter-electrodes, which significantly reduced the open area of the gaps and thus restricted the flow in and out of the electrode zone, as shown in Figure 8.

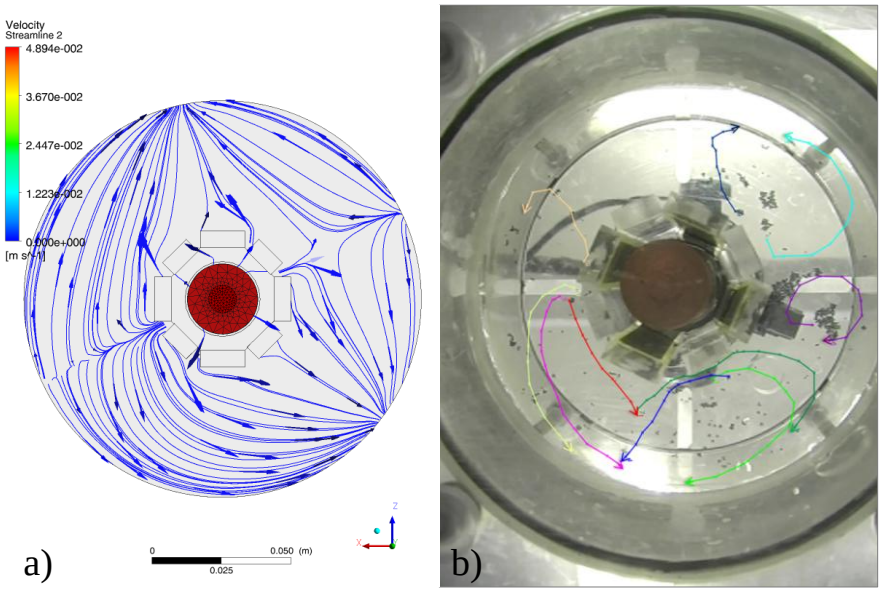

Figure 8. Stream lines for reactor *c*.

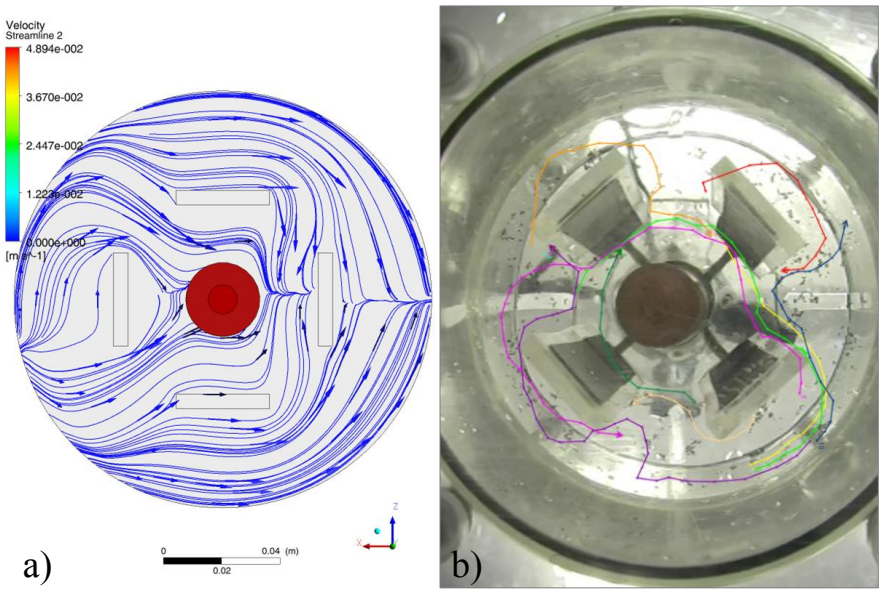

Figure 9. Stream lines for reactor *d*.

The main stream flow in reactor *c* is in the periphery of the tank, whereas the flow in the electrode zone is not replaced by new electrolytes. The experimental and simulated results show that configuration *c* promotes a stagnant fluid zone between the copper electrode and counter electrode. This phenomenon significantly reduces the contact between the electrolyte and electrodes, lowering the capacity of the reactor. Thus, this configuration is expected to produce a low efficiency.

In contrast, increasing the amount of contact between the electrolyte and electrodes can increase the efficiency. In reactor *d*, the gap between the counter electrodes was modified (Figure 9).The electrolyte flows without restraints into the reaction zone, and the rotating cylinder is transferring enough momentum to keep the electrolyte flowing. This configuration shows a possible increase in the efficiency of the reactor. The only part missing from this study is the limit current analysis to ensure that geometry d is the optimum configuration explored in this work.

5. CONCLUSIONS

Computational fluid dynamics (CFD) is a very useful design tool for characterizing the dynamics of the flow in electrochemical reactors at a very low cost. CFD can be easily applied to scale up any of the reactors presented in this work. The variations in the flow produced by the change in the counter electrode configuration show that the electrochemical process can be significantly affected and that a full characterization of the dynamics of the electrolyte is mandatory.

The gap between the counter electrodes determines the stream lines of the electrode. In reactor *c*, the reduction in the gap causes stagnant flow in the reaction zone, limiting the efficiency of the process and thus preventing the reaction products from being transported out of the reaction zone. In geometry *d*, the open area between the counter electrodes allows for the free flow of the electrolyte through the reaction zone, producing more efficient transport of the reaction products. It can be concluded that CFD can be applied to characterize the flow in electrochemical rotating cylinder reactors and to explore novel designs that can lead into increased efficiency.

ACKNOWLEDGMENTS
The authors are grateful for the financial support from CONACYT provided through the project CB-154774. R. Enciso is grateful for the scholarship granted.

References

1. J. M. Grau and J. M. Bisang, *J. Appl. Electrochem.*, 37 (2007) 275.
2. F. F. Rivera, I. González and J. L. Nava, *Environ. Technol.*, 29 (2008) 817.
3. S. Matlalcuatzi and J. L. Nava, *Water Sci. Technol.*, 65 (2012) 1406.
4. E. M. Elsayed and A. E. Saba, *Int. J. Electrochem. Sci.*, 4 (2009) 627.
5. F. F. Rivera, J. L. Nava, M. T. Oropeza, A. Recéndiz and G. Carreño, *Electrochim. Acta*, 55 (2010) 3275.
6. E. P. Rivero, P. Granados, F. F. Rivera, M. Cruz and I. González, *Chem. Eng. Sci.*, 65 (2010) 3042.
7. J. A Delgadillo, R. Enciso, C. Ojeda and I. Rodríguez, *Int. J. Electrochem. Sci.*, 7 (2012) 2065.

8. R. Thilakavathi, D. Rajasekhar, N. Balasubramanian, C. Srinivasakannan and A. Al Shoaibi, *Int. J. Electrochem. Sci.*, 7 (2012) 1386.
9. S. Martinez-Delgadillo, H. Mollinedo-Ponce, V. Mendoza-Escamilla, C. Gutierrez-Torres, J. Jimenez-Bernal and C. Barrera-Diaz, *J. Clean. Prod.*, 34 (2012) 120.
10. F. Tomasoni, J.F. Thomas, D. Yildiz, J. van Beeck and J. Deconinck, *WIT Transactions on Engineering Sciences*, 54 (2007) 153.
11. J. A. Delgadillo and R. Rajamani, *Int. J. Miner. Processing*, 77 (2005) 217.
12. D. Choudhury, D, *Introduction to the renormalization group method and turbulence modeling*. Fluent Inc. Technical Memorandum TM-107 (1993).
13. A. J. Odgaard, *J. Hydraul. Eng.*, 4 (1986) 610.